

# Non-thermal hot electrons ultrafastly generating hot optical phonons in graphite

Y. Ishida,<sup>1,2</sup> T. Togashi,<sup>2</sup> K. Yamamoto,<sup>2,3</sup> M. Tanaka,<sup>1</sup>  
T. Taniuchi,<sup>1</sup> T. Kiss,<sup>1</sup> M. Nakajima,<sup>1</sup> T. Suemoto,<sup>1</sup> and S. Shin<sup>1,2,4</sup>

<sup>1</sup>ISSP, University of Tokyo, Kashiwa, Chiba 277-8581, Japan

<sup>2</sup>RIKEN SPring-8 Center, Sayo, Hyogo 679-5148, Japan

<sup>3</sup>Graduate School of Engineering, Osaka Prefecture University, Sakai, Osaka 599-8531, Japan

<sup>4</sup>CREST, Japan Science and Technology Agency, Tokyo 102-0075, Japan

Ultrafast dynamics of graphite is investigated by time-resolved photoemission spectroscopy. We observe spectral features of direct photoexcitations, non-thermal electron distributions, and recovery dynamics occurring with two time scales having distinct pump-power dependences. Additionally, we find an anomalous increase of the spectral intensity around the Fermi level, and we attribute this to spectral broadenings due to coupled optical phonons in the transient. The fingerprints of the coupled optical phonons occur from the temporal region where the electronic temperature is still not definable. This implies that there is a mechanism of ultrafast-and-efficient phonon generations beyond a two-temperature model.

Investigation of the non-equilibrium dynamics after an impulsive impact provides insights into couplings among various excitations. A two-temperature model (TTM) is often a starting point to understand the coupled dynamics of electrons and lattice vibrations: the optical pulse primarily raises the electronic temperature  $T_{el}$  while leaving the lattice temperature  $T_l$  low; subsequently the hot electrons heat up the lattice until  $T_{el} = T_l$  is reached. This temporal hierarchy owes to the assumption that the electron-electron scattering rate is much larger than the electron-phonon scattering rate. We report herein that the TTM scheme is seriously invalidated in semimetal graphite. Time-resolved photoemission spectroscopy (TrPES) of graphite reveals that fingerprints of coupled optical phonons (COPs) occur from the initial moments where  $T_{el}$  is still not definable. Our study shows that ultrafast-and-efficient phonon generations occur beyond the TTM scheme, presumably associated to the long duration of the non-thermal electrons in graphite.

One of the most interesting observation in the ultrafast dynamics of graphite is that  $T_{el}$  in the sub-picosecond temporal region stays somewhat low even though irradiated with an intense femtosecond optical pulse [1]. This led to the picture that the electronic energy is quasi-instantaneously transferred to the COPs through strong electron-phonon couplings [1] based on the TTM scheme [2, 3, 4]. However, electron-phonon coupling constant is reported to be moderately small in graphite [6], making the mechanism of the ultrafast COP generation elusive. Subsequent studies also suggest the nearly instantaneous COP generation coupled to the electron dynamics [7, 8, 9, 10, 11, 12, 13, 14], which is considered to affect ballistic transports at high fields [15, 16, 17, 18, 19]. Nevertheless, direct observation of the electron distribution in the transient is limited [9, 12, 20, 21], and more-

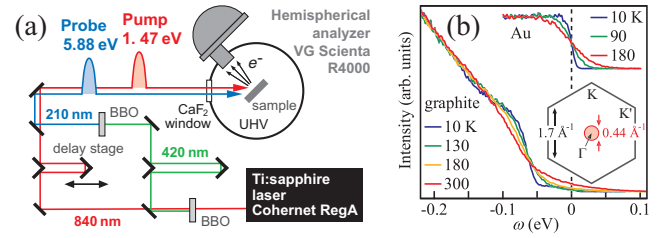


FIG. 1: TrPES system. (a) A schematic of the TrPES system. (b) Spectra of graphite recorded in normal-emission geometry. The increase of the intensity at  $E_F$  with increasing  $T$  is due to the increased population of the COPs [5]. Inset of (b) shows the surface Brillouin zone of graphite, and the area probed in the normal-emission geometry is indicated by a circle.

over, simultaneous detection of the electron distribution and the phonons in the transient has been beyond reach. TrPES [Fig. 1(a)] is one of the most powerful tools to investigate the dynamics of the electrons, since it can provide information of the transient electron distributions in a wide energy range across the Fermi level ( $E_F$ ) [4, 20, 21, 22, 23, 24]. Furthermore, Liu *et al.* [5] recently reported that fingerprints of COPs occur in the photoemission spectra of graphite, as we shall explain below. Therefore, it became possible to monitor simultaneously the electron distribution and the fingerprints of COPs during the ultrafast dynamics of graphite by TrPES.

The fingerprints of COPs show up in the spectra recorded in a normal-emission geometry [5], that is, when we detect the photoelectrons around  $\Gamma$  of the surface Brillouin zone of graphite [inset in Fig. 1(b)]. Since there are no bands around  $\Gamma$  in the vicinity of  $E_F$ , the signal consists of photoelectrons around  $K$  ( $K'$ ) indirectly scattered into the vicinity of  $\Gamma$  mainly by phonons. As we shall see later, signals of direct photoexcitations around the  $K$  ( $K'$ ) point indeed occur in the TrPES spectra recorded in the normal-emission geometry. A gap-like feature of  $\sim 70$  meV occurs in the spectra near- $E_F$

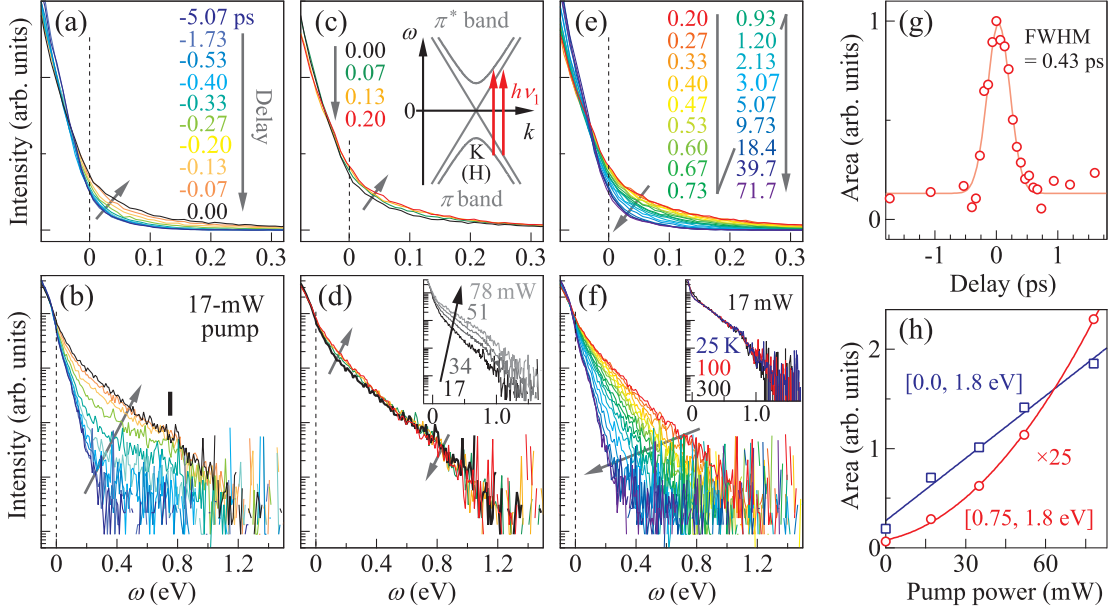


FIG. 2: TrPES of graphite Spectra recorded at 17-mW pump at  $t \leq 0$  ps (a, b),  $0 \leq t \leq 0.2$  ps (c, d), and  $t \geq 0.2$  ps (e, f). Here, (b, d, f) are semi-logarithmic plots of (a, b, c), respectively. Insets in (d) and (f) show spectra at  $t = 0$  ps recorded at various pump powers and temperatures, respectively. (g) Spectral weight between 0.8-1.0 eV as a function of  $t$  overlaid with a Gaussian. (h) Spectral weight under 0.75-1.8 eV (above the cutoff; circle) and under 0.0-1.8 eV (in the unoccupied side; square) at  $t = 0$  ps as a function of pump power overlaid with first and second order polynomial functions, respectively. The schematic in (c) shows direct excitations from the  $\pi$  bands to the  $\pi^*$  bands.

at low  $T$  [Fig. 1(b)], since phonon absorption process is quenched and phonon emission (energy-loss) process dominates. With increasing  $T$ , phonon absorption process is increased, and the spectral weight tails into higher energies resulting in an increase of the spectral intensity at  $E_F$  [Fig. 1(b)]. This is similar to anti-Stokes lines in Raman spectra gaining stronger intensity at higher temperatures. Thus, we utilize the spectral intensity at  $E_F$  in TrPES as a measure of the number of COPs in the transient. The optical phonons monitored herein are assigned to the 67-meV out-of-plane and the  $\sim 150$ -meV in-plane modes [5].

**Results.**— Figure 2(a-f) show TrPES spectra of graphite,  $I(\omega, t)$ , recorded under a pump power  $p = 17$  mW (a fluence of  $\sim 14 \mu\text{J}/\text{cm}^2$ ) at room temperature. A movie file is provided in Supplementary Information. Overall, we observe that the electrons are pumped from the occupied side to the unoccupied side and subsequent recovery dynamics lasting over several tens of picoseconds: at  $t \leq 0$  ps, the spectral intensity  $I(\omega, t)$  is increased in the unoccupied side; at  $0 \leq t \leq 0.20$  ps,  $I(\omega, t)$  at  $\omega \sim 0.75$  eV is decreased, whereas that at  $\omega \sim 0$  eV is increased; at  $t \geq 0.20$  ps,  $I(\omega, t)$  in the unoccupied side is decreased. Here,  $t = 0$  ps has been determined utilizing the fast response of  $\sim 20$  fs observed at  $\omega > 0.8$  eV [12], and the time resolution [full width at half the maximum (FWHM)] is estimated to be  $\Delta t = 0.43$  ps, see Fig. 2(g).

We observe a plateau feature in the unoccupied side during the pump [Fig. 2(b) and the movie file in Supplementary Information], which is a hallmark of a non-thermal electron distribution [22]. The plateau turns over into an exponential tailing at  $t \gtrsim 0.20$  ps [Fig. 2(f)], indicating that the electrons are distributed according to the Fermi-Dirac function. That is, electronic thermalization occurs at  $\tau_e \sim 0.2$  ps so that  $T_{el}$  becomes definable thereafter. In metallic materials, typical time scale for electronic thermalization is considered to be  $\tau_e \sim 10$  fs or less [2], and if  $\Delta t \gg \tau_e$ , one would not expect to observe a non-thermal distribution of the hot electrons. In fact, in the TrPES study of a metallic  $\text{Bi}_2\text{Sr}_2\text{CaCu}_2\text{O}_{8+\delta}$  [4], Perfetti *et al.* observed with  $\Delta t \sim 90$  fs that the spectra mostly obey Fermi-Dirac statistics even at  $t \sim 0$  ps. The smallness of  $1/\tau_e$  in graphite can be attributed to the semimetallic band structure: Since electronic states near  $E_F$  occur only around  $K(K')$  points of the surface Brillouin zone, the available phase space for electron-electron scatterings becomes vanishingly small in approaching  $E_F$  particularly after the initial avalanche of the hot electrons towards  $E_F$ . This can act as a bottleneck for the non-thermal electrons to relax into the thermal (Fermi-Dirac) distribution.

The plateau observed just after the pump extends up to a cutoff at  $\omega \sim 0.75$  eV, as indicated by a bar in Fig. 2(b). This cutoff can be understood as a fingerprint of di-

rect photoexcitations occurring around the  $K(K')$  point: since the  $\pi$ - and  $\pi^*$ -bands are nearly symmetric about  $E_F$  as shown in the schematic in Fig. 2, direct excitations are dominated by the transitions from  $\omega = -\hbar\nu_1/2$  to  $+\hbar\nu_1/2$ , and therefore, the cutoff energy can be identified to  $\omega \sim \hbar\nu_1/2 = 0.75$  eV. Note that such a fingerprint of direct excitations would not be detected if  $\tau_e \ll \Delta t$ . Therefore the  $\sim 0.75$ -eV cutoff strengthens the conclusion that the duration of the non-thermal electron distribution is detected in the present study.

With increasing  $p$ , the cutoff is blurred [inset in Fig. 2(d)], so that the unoccupied side of the spectra becomes featureless and the line shape becomes similar to the TR-PES spectra of graphite reported previously [21]. The intensity above the cutoff at  $t = 0$  ps grows quadratically with  $p$  while the intensity in the unoccupied side grows linearly with  $p$  [Fig. 2(h)]. The latter indicates that the number of electrons excited by the pump is proportional to  $p$  at least up to 78 mW, whereas the former indicates that the excited electrons are further scattered above the cutoff by other excitations such as the hot electrons themselves or hot phonons, since such scatterings occur roughly proportional to the square of the population of the excited particles. The intensity and the sharpness of the cutoff are almost independent of  $T$  [inset of Fig. 2(f)], indicating that the blurring of the cutoff is not related to the thermally populated excitations in the initial state.

We now turn to the variation of the spectral weight around  $E_F$ , which serves as the fingerprints of COPs in the transient, as explained previously. One can see that the variation starts from the beginning of the transient in accord with the reports of the nearly instantaneous generation of the COPs in graphite [8, 11, 14]. Our findings therefore show that the ultrafast COP generation takes place from the temporal region where the hot electrons are not thermalized [see, Fig. 2(a) and the movie file in Supplementary Information]. After  $t \sim 0.2$  ps, the intensity at  $E_F$  starts to decrease, see Fig. 2(e), indicating that the COP generation is mostly accomplished within  $t \lesssim 0.2$  ps. The results are in strong contrast to the TTM scheme, where COPs are assumed to be cool at the beginning and then gradually heated up by the electrons that are thermalized.

**Analysis.**— First, we investigate how the total electronic energy dissipates with time. As  $I(\omega, t)$  reflects the occupied density of states (DOS),  $\int_0^\infty \omega \Delta I(\omega, t) d\omega$  is a measure of the excess electronic energy, and we plot this as a function of  $t$  in Fig. 3(a). Here,  $\Delta I(\omega, t) = I(\omega, t) - I(\omega, -5 \text{ ps})$ . The energy dissipation occurs with two time scales having distinct pump-power dependences: at  $t \lesssim 1$  ps, the energy dissipation rate positively depends on  $p$ , whereas at  $t \gtrsim 1$  ps, it is independent of  $p$ . The fast dynamics at  $t \lesssim 1$  ps is attributed to the net energy flow from the hot electrons to the hot COPs through electron-phonon scatterings, since this

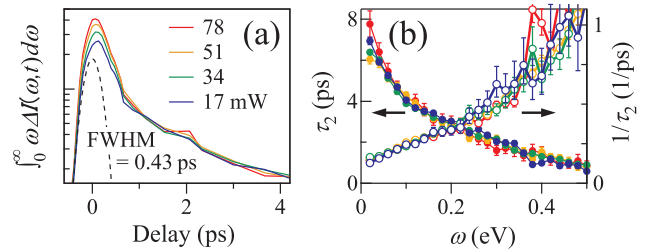


FIG. 3: Decay rates. (a) Electronic energy (see text) *vs t* for various pump powers. Each curve has an arbitrary offset. Dashed line represents the time resolution. (b) The spectra of decay time and decay rate (left and right axes, respectively) of the slow component.

channel is increased quadratically with  $p$  due to the increased populations of the hot electrons and hot COPs. Note that the scatterings among the hot electrons cannot account for the loss of the electronic energy [25]. At  $t \sim 1$  ps, the electrons and COPs reach quasi-equilibrium ( $T_{el} = T_{COP}$ ) after a sufficient number of scatterings, and the electron-COP composite dissipates its energy to the heat bath such as acoustic phonons [26], and hence the  $p$ -independent energy dissipation at  $t \gtrsim 1$  ps.

Further analysis of the spectra also supports that the recovery dynamics at  $t \gtrsim 1$  ps is characterized by  $T_{el} = T_{COP}$  and decay rates independent of  $p$ . First, we derive the decay-rate spectrum for the slower component  $1/\tau_2(\omega)$ , which is obtained by fitting  $I(\omega, t)$  at each energy with a double exponential function (Supplementary Information). As shown in Fig. 3(b),  $1/\tau_2(\omega)$  is independent of  $p$  and is quasi-linear to  $\omega$  at  $\omega \lesssim 0.3$  eV. Second, we quantify the spectral shape by simulating the spectrum as  $I(\omega, t) = a(t) \int G(\omega - \omega', \sigma^2(t) + \sigma_R^2) D(\omega') f(\omega', T_{el}(t)) d\omega'$ . Here,  $G(\omega, \sigma^2 + \sigma_R^2)$  is a Gaussian with FWHM of  $\sqrt{\sigma^2 + \sigma_R^2}$ ,  $f(\omega, T_{el})$  is the Fermi-Dirac function,  $a(t)$  is a scaling factor, and  $D(\omega)$  is a DOS. The Gaussian broadening accounts for the spectral weight accumulating from lower energies, so that  $\sigma^2$  becomes a measure of the number of the COPs in the transient. The spectra are nicely reproduced throughout the transient [Fig. 4(a) and Supplementary Information], and the fitting parameters are summarized in Fig. 4(b) and 4(c). One can see that  $\sigma^2$  and  $a$  for  $t > 1.0$  ps scales with  $T_{el}$  and does not explicitly depend on  $p$ . This indicates that the number of the COPs at  $t > 1.0$  ps is a function of  $T_{el}$ , i.e.,  $T_{COP} = T_{el}$ , and that the spectral shape at  $t > 1.0$  ps is determined only by  $T_{el}$ , which is the temperature of the electron-COP composite.

**Discussion.**— We experimentally find that the electronic distribution is non-thermal at  $t \lesssim 0.2$  ps, and also find evidence that the COP generation is mostly accomplished within this initial temporal region. This strongly indicates that the mechanism of the ultrafast COP gen-

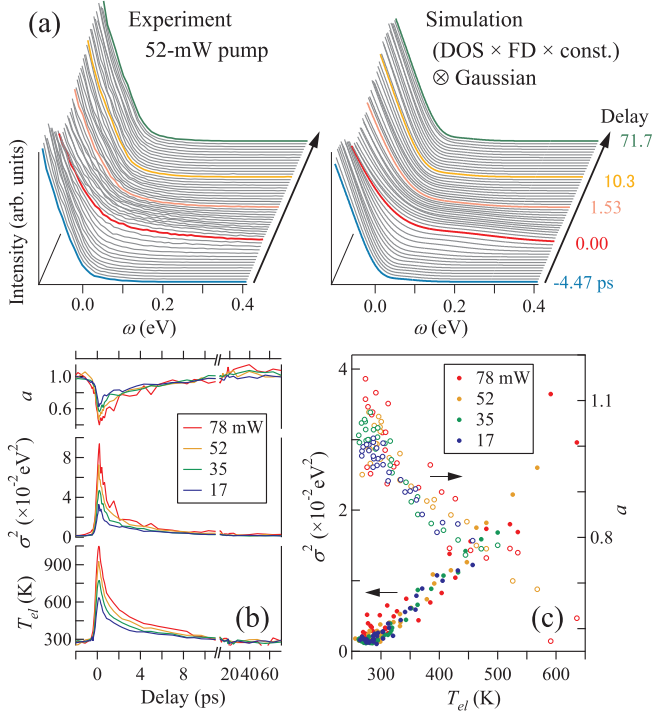


FIG. 4: Optical-phonon broadenings during the transient. (a) TrPES spectra recorded under 52-mW pump (left) and the simulated spectra (right). (b) Fitting parameters. (c) A plot of the fitting parameters  $\sigma^2$  and  $a$  with respect to  $T_{el}$  for  $t > 1.0$  ps.

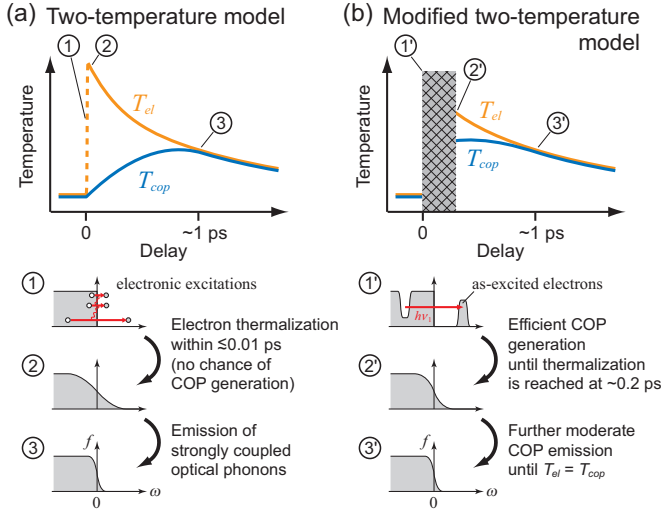


FIG. 5: Two-temperature model (a) and beyond (b). The top panels show the transient change of  $T_{el}$  and  $T_{cop}$ . Hatched area indicates temporal region where  $T_{el}$  cannot be defined. The lower panels show electron distribution functions ( $f$ ) at some selected moments. The major difference in the COP-generation mechanism between the two is whether they are generated by the thermal electrons (a) or by the non-thermal electrons (b).

eration is beyond the TTM scheme, see Fig. 5. Since the duration of the non-thermal electron distribution is longer than that in the TTM scheme, the high-energy electrons, which is considered to be favorable for generating high-energy COPs [27], indeed have more chance to generate COPs before they degrade into low-energy thermalized electrons. Therefore, not only the largeness of the electron-phonon couplings but also the long durations of the non-thermal electron distribution may be crucial for understanding the ultrafast-and-efficient generation of the COPs in graphite. It is interesting to note that a break-down of TTM was also suggested in  $\text{YBa}_2\text{Cu}_3\text{O}_{7-\delta}$  [28], in which the DOS becomes vanishingly small around  $E_F$  in the  $d$ -wave superconducting state, similar to the case for graphite. Therefore, coupled dynamics directly involving the non-thermal electrons may be sought in materials that have vanishingly small DOS around  $E_F$ , for example in neutral graphene [29], in nodal superconductors [28], and on the surface of topological insulators [30]. Alternatively, we do not exclude the possibility that the hot COPs and hot electrons are co-generated by the pump, which may be viewed as a counterpart of the breakdown of adiabatic Born-Oppenheimer approximation [31]: in as much as the electrons cannot follow the motion of the lattice, COPs are simultaneously generated when the electronic excitation takes place. Whichever the case may be, our study reveals that there is a unique mechanism of ultrafast COP generation where the concept of temperatures is broken.

**Methods.**— The TrPES apparatus consists of an amplified Ti:sapphire laser system delivering  $h\nu_1 = 1.5$  eV pulses of 170-fs duration with 250-kHz repetition and a hemispherical analyzer [32], see Fig. 1(a). A portion of the laser is converted into  $h\nu_4 = 5.9$  eV probing pulses using two non-linear crystals,  $\beta\text{-BaB}_2\text{O}_4$  (BBO), and the time delay  $t$  from the pump is controlled by a delay stage. The pump and probe pulses are  $p$ -polarized and have spot diameters of  $\sim 0.8$  and  $\sim 0.3$  mm, respectively, at the sample position. The intensity of the probe pulse is minimized to avoid space charge effects. Multi-photon photoemission due to the pump pulse is not observed in the dataset presented herein.  $E_F$  is referenced to the Fermi cutoff of gold and the energy resolution  $\sigma_R$  is 11 meV. The base pressure of the photoemission chamber is  $1 \times 10^{-10}$  Torr, and highly-oriented pyrolytic graphite is cleaved *in situ*.

- 
- [1] Kampfrath, T., Perfetti, L., Schapper, F., Frischkorn, C. & Wolf, M. Strongly coupled optical phonons in the ultrafast dynamics of the electronic energy and current relaxation in graphite. *Phys. Rev. Lett.* **95**, 187403 (2005).
  - [2] Allen, P. B. Theory of thermal relaxation of electrons in metals. *Phys. Rev. Lett.* **59**, 1460-1463 (1987).
  - [3] Brorson, S. D. *et al.* Femtosecond room-temperature



- measurement of the electron-phonon coupling constant  $\lambda$  in metallic superconductors. *Phys. Rev. Lett.* **64**, 2172-2175 (1990).
- [4] Perfetti, L. *et al.* Ultrafast electron relaxation in superconducting  $\text{Bi}_2\text{Sr}_2\text{CaCu}_2\text{O}_{8+\delta}$  by time-resolved photoelectron spectroscopy. *Phys. Rev. Lett.* **99**, 197001 (2007).
- [5] Liu, Y. *et al.* Phonon-induced gaps in graphene and graphite observed by angle-resolved photoemission. *Phys. Rev. Lett.* **105**, 136804 (2010).
- [6] Leem, C. S. *et al.* Effect of linear density of states on the quasiparticle dynamics and small electron-phonon coupling in graphite. *Phys. Rev. Lett.* **100**, 016802 (2008).
- [7] Dawlaty, J. M., Shivaraman, S., Chandrashekar, M., Rana, F. & Spencer, M. G. Measurement of ultrafast carrier dynamics in epitaxial graphene. *Appl. Phys. Lett.* **92**, 042116 (2008).
- [8] Ishioka, K. *et al.* Ultrafast electron-phonon decoupling in graphite. *Phys. Rev. B* **77**, 121402 (2008).
- [9] Sun, D. *et al.* Ultrafast relaxation of excited Dirac fermions in epitaxial graphene using optical differential transmission spectroscopy. *Phys. Rev. Lett.* **101**, 157402 (2008).
- [10] Luer, L. *et al.* Coherent phonon dynamics in semiconducting carbon nanotubes: A quantitative study of electron-phonon coupling. *Phys. Rev. Lett.* **102**, 127401 (2009).
- [11] Yan, H. *et al.* Time-resolved Raman spectroscopy of optical phonons in graphite: Phonon anharmonic coupling and anomalous stiffening. *Phys. Rev. B* **80**, 121403 (2009).
- [12] Breusing, M., Ropers, C. & Elsaesser, T. Ultrafast carrier dynamics in graphite. *Phys. Rev. Lett.* **102**, 086809 (2009).
- [13] Wang, H. *et al.* Ultrafast relaxation dynamics of hot optical phonons in graphene. *Appl. Phys. Lett.* **96**, 081917 (2010).
- [14] Kang, K., Abdula, D., Cahill, D. G. & Shim, M. Lifetimes of optical phonons in graphene and graphite by time-resolved incoherent anti-Stokes Raman scattering. *Phys. Rev. B* **81**, 165405 (2010).
- [15] Yao, Z., Kane, C. L. & Dekker, C. High-field electrical transport in single-wall carbon nanotubes. *Phys. Rev. Lett.* **84**, 2941-2944 (2000).
- [16] Chae, D.-H., Krauss, B., von Klitzing, K. & Smet, J. H. Hot phonons in an electrically biased graphene constriction. *Nano Lett.* **10**, 466-471 (2010).
- [17] Hwang, H., Hu, B. Y. K. & Sarma, S. D. Inelastic carrier lifetime in graphene. *Phys. Rev. B* **76**, 115434 (2007).
- [18] Calandra, M. & Mauri, F. Electron-phonon coupling and electron self-energy in electron-doped graphene: Calculation of angular-resolved photoemission spectra. *Phys. Rev. B* **76**, 205411 (2007).
- [19] Tse, W.-K., Hwang, E. H. & Sarma, S. D. Ballistic hot electron transport in graphene. *Appl. Phys. Lett.* **93**, 023128 (2008).
- [20] Xu, S. *et al.* Energy dependence of electron lifetime in graphite observed with femtosecond photoemission spectroscopy. *Phys. Rev. Lett.* **76**, 483-486 (1996).
- [21] Moos, G., Gahl, C., Fasel, R., Wolf, M. & Hertel, T. Anisotropy of quasiparticle lifetimes and the role of disorder in graphite from ultrafast time-resolved photoemission spectroscopy. *Phys. Rev. Lett.* **87**, 267402 (2001).
- [22] Fann, W. S., Storz, R., Tom, H. W. K. & Bokor, J. Electron thermalization in gold. *Phys. Rev. B* **46**, 13592-13595 (1992).
- [23] Perfetti, L. *et al.* Time evolution of the electronic structure of 1T-TaS<sub>2</sub> through the insulator-metal transition. *Phys. Rev. Lett.* **97**, 067402 (2006).
- [24] Schmitt, F. *et al.* Transient electronic structure and melting of a charge density wave in TbTe<sub>3</sub>. *Science* **321**, 1649-1652 (2008).
- [25] Tse, W.-K. & Sarma, S. D. Energy relaxation of hot Dirac fermions in graphene. *Phys. Rev. B* **79**, 235406 (2009).
- [26] Bistrizter, R. & MacDonald, A. H. Electronic cooling in graphene. *Phys. Rev. Lett.* **102**, 206410 (2009).
- [27] Butscher, S., Milde, F., Hirtschulz, M., Malic, E. & Knorr, A. Hot electron relaxation and phonon dynamics in graphene. *Appl. Phys. Lett.* **91**, 203103 (2007).
- [28] Pashkin, A. *et al.* Femtosecond response of quasiparticles and phonons in superconducting  $\text{YBa}_2\text{Cu}_3\text{O}_{7-\delta}$  studied by wideband terahertz spectroscopy. *Phys. Rev. Lett.* **105**, 067001 (2010).
- [29] Novoselov, K. S. *et al.* Electric Field Effect in Atomically Thin Carbon Films. *Science* **306**, 666-669 (2004).
- [30] Hasan, M. Z. & Kane, C. L. Topological insulators. *Rev. Mod. Phys.* **82**, 3045-3067 (2010).
- [31] Pisana, S. *et al.* Breakdown of the adiabatic Born-Oppenheimer approximation in graphene. *Nature Mater.* **6**, 198-201 (2007).
- [32] Kiss, T. *et al.* A versatile system for ultrahigh resolution, low temperature, and polarization dependent Laser-angle-resolved photoemission spectroscopy. *Rev. Sci. Instrum.* **79**, 023106 (2008).